Probing structure in invisible protein states with anisotropic NMR chemical shifts

Pramodh Vallurupalli, D. Flemming Hansen, and Lewis E. Kay

Departments of Medical Genetics, Biochemistry and Chemistry, University of Toronto, Toronto, Ontario, Canada, M5S 1A8

Supplementary Figure 1: ^{13}C' relaxation dispersion experiment used for measuring ^{iso} and ^{aniso}.

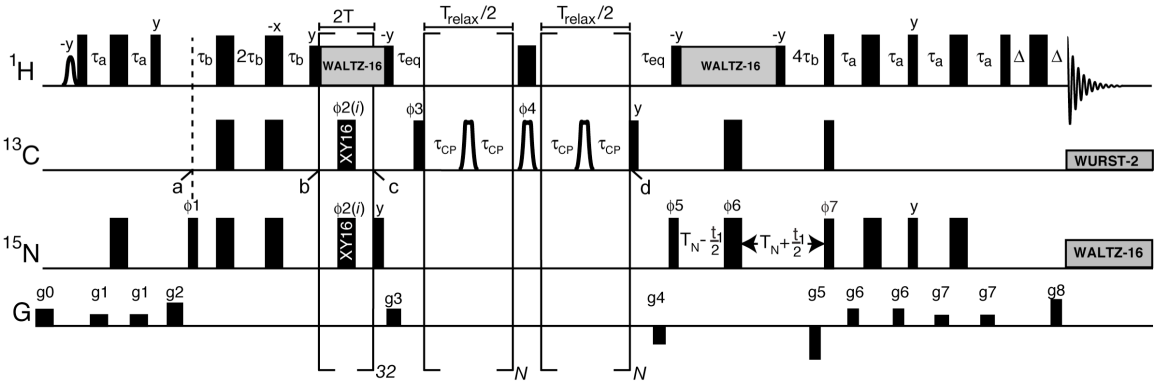

Pulse scheme of the ^{13}C' constant-time relaxation dispersion experiment for measuring millisecond time-scale dynamics in ^{15}N-, ^{13}C'-labeled proteins. ^{1}H, ^{13}C, and ^{15}N 90º (180º) rf pulses are shown as narrow (wide) black bars; ^{1}H and ^{15}N pulses are applied at the highest possible power level, while ^{13}C pulses (both those that are rectangular and the shaped RE-BURP[1] pulses during the CPMG element between points *c* and *d*) are applied with a 16 kHz field. The use of ^{13}C'-selective pulses during the CPMG element refocuses small (2 or more bond) ^{13}C'-aliphatic carbon couplings that arise from the labeling scheme employed. The shaped 90º ^{1}H pulse of phase –y is water-selective (~1.6 ms rectangular pulse). All pulse phases are assumed to be x, unless indicated otherwise. The ^{1}H carrier is placed on the water signal, while the ^{13}C and ^{15}N rf carriers are at 176 and 119 ppm, respectively. Magnetization transfer from ^{15}N to ^{13}C' occurs from *a* to *c*; from *a* to *b* ($0.5/J_{NH}$) ^{15}N magnetization is refocused with respect to ^{1}H and dephased with respect to ^{13}C'. Subsequently, from *b* to *c*, ^{15}N evolution with respect to the one-bond ^{15}N-^{13}C' scalar coupling continues through the application of simultaneous ^{13}C and ^{15}N pulses at a frequency of 800 Hz. This scheme quenches chemical exchange that occurs on time-scales slower than ~ 1/800 Hz ~ 1.3 ms leading to improvements in sensitivity[2,3]. Each of the simultaneous 32 pulses labeled XY 16 has phase

2(*i*)=2{x,y,x,y,y,x,y,x, x, y, x, y, y, x, y, x}^{4} (*i.e.*, pulse 1 is phase x, pulse 2 phase y, pulse 3 phase x, *etc.*) so that both the x and the y components of transverse magnetization are refocused properly in the presence of off-resonance effects and pulse imperfections. ^{1}H decoupling during the ^{15}N --> ^{13}C' transfer and during t_1 is achieved with a WALTZ-16 scheme[5] applied at a field of 6 kHz. ^{15}N decoupling during acquisition is achieved with a 1.5 kHz WALTZ-16 scheme while a WURST-2 ^{13}C' decoupling scheme is employed during acquisition to suppress ^{1}HN-^{13}C' scalar/dipolar couplings (bandwidth of 12 ppm, centered at 175 ppm, maximum(rms) B_1 field of 0.5(0.3) kHz). The phase cycling used is: 1 = {y, y}, 3=2{y},2{ y}, 4={y, y}, 5={x}, 6=4{x},4{ x}, 7={x}, receiver={x, x, x,x}. The delays used are $_a$ = 2.25 ms, $_b$ = 1/(8J_{NH}) ~1.38 ms, $_{eq}$ = 5 ms, T = 10 ms, T_N = 13 ms and = 0.5 ms. *N* is any whole number. Gradient strengths G/cm (length in ms) are: g0=8.0(0.5), g1=4.0(0.5), g2=10.0(1.0), g3=7.0(1.0), g4= 6.0(0.6), g5= -30.0(1.25), g6=4.0(0.3), g7=2.0(0.4), g8=29.6(0.125). Quadrature detection in the indirect dimension is obtained by recording two sets of spectra with (7,g5) and (7+ ,-g5) for each t_1 increment[6,7]; the phase 5 is incremented along with the receiver by 180° for each complex t_1 point[8]. The inter-residue 2-bond ^{1}HN-^{13}C' scalar coupling is ≤ 4 Hz but under the conditions of alignment used here the corresponding dipolar coupling can be on the order of 10 Hz (ref [9]). Thus, the effective ^{13}C' chemical shifts for those spins coupled to ^{1}HN in the up/down position differ by as much as 10 Hz. In principal, the ^{13}C' signal is comprised of magnetization from essentially equal numbers of ^{1}HN spins up or down so that to first order values of extracted from dispersion profiles should be independent of the 2-bond ^{1}HN-^{13}C' coupling. The ^{1}H 180° pulse applied simultaneously with ^{13}C $180^o{}_4$ interchanges ^{1}HN spin states after the first half of the T_{relax} period that effectively averages out the effects of the coupling. This can also be achieved (more

rigorously) through continuous ^{1}H decoupling during this interval, although we have not attempted this here.

Supplementary Table 1: List of $\Delta\omega^{iso}$, $\Delta\omega^{aniso}$, $\Delta\omega_A$ and $\Delta\omega_B$ values[a].

Residue	$\Delta\omega^{aniso}$	error	$\Delta\omega^{iso}$	error	$\Delta\omega_A$(direct)	error	$\Delta\omega_B$(direct)[b]	error	$\Delta\omega_B$[c]	error
ALA 6	0.215	0.011	0.101	0.019	-0.039	0.001	-0.111	0.002	-0.153	0.022
GLU 7	0.151	0.015	0.132	0.019	-0.047	0.002	-0.040	0.009	-0.066	0.024
TYR 8	0.225	0.011	0.255	0.010	0.005	0.000	0.039	0.001	0.035	0.015
ASP 9	0.287	0.010	0.190	0.012	0.015	0.003	-0.059	0.009	-0.082	0.016
ALA 13	-0.183	0.013	-0.320	0.010	-0.075	0.001	-0.159	0.002	-0.212	0.016
ASP 15	0.326	0.011	0.424	0.010	-0.031	0.003	0.073	0.004	0.067	0.015
PHE 31	-0.587	0.015	-0.463	0.011	0.026	0.002	0.129	0.002	0.150	0.019
VAL 32	1.844	0.040	1.756	0.039	-0.031	0.002	-0.115	0.001	-0.119	0.056
ASP 34	0.251	0.011	0.231	0.010	0.014	0.004	0.002	0.009	-0.005	0.015
TRP 36	0.482	0.013	0.411	0.010	-0.083	0.004	-0.087	0.001	-0.154	0.017
TRP 37	-0.390	0.010	-0.382	0.010	-0.070	0.002	-0.054	0.000	-0.062	0.014
SER 52	0.786	0.021	0.607	0.013	-0.090	0.001	-0.186	0.006	-0.269	0.024
ASN 53	0.473	0.012	0.481	0.011	0.071	0.002	0.058	0.005	0.079	0.016
TYR 54	-0.340	0.010	-0.282	0.010	-0.058	0.001	0.003	0.002	0.000	0.014

a $\Delta\omega^{iso} = \Delta\omega^{iso}_{P} - \Delta\omega^{iso}_{PL}$, $\Delta\omega^{aniso} = \Delta\omega^{aniso}_{P} - \Delta\omega^{aniso}_{PL}$, $\Delta\omega_A = \Delta\omega^{aniso}_{P} - \Delta\omega^{iso}_{P}$ and $\Delta\omega_B = \Delta\omega^{aniso}_{PL} - \Delta\omega^{iso}_{PL}$.

b $\Delta\omega_B$(direct) values were calculated directly from spectra of the fully ligated sample.

c $\Delta\omega_B$ values of the invisible state were calculated from the relation $\Delta\omega_B = \Delta\omega^{iso} + \Delta\omega_A \cdot \Delta\omega^{aniso}$, using chemical shift differences measured on the 7% ligand bound sample.

Supplementary Methods

Protein Production and NMR Samples: ^{15}N, $^{13}C'$, ^{2}H-labeled Abp1p SH3 domain[10-12] was prepared by growth in *E. coli*. BL21(DE3) cells, as described previously[13]. Labeling was achieved using 2.5 g/L [1-^{13}C]-pyruvate and 5 mM (~0.5 g/L) $NaH^{13}CO_3$ as the carbon sources, ^{15}N ammonium chloride as the nitrogen source and the growth was performed in 99.9% $^{2}H_2O$ (manuscript in preparation). The culture was grown to OD ~ 0.8 and then induced with 1 mM IPTG. At this point another 5 mM $NaH^{13}CO_3$ was added. An analysis to be presented elsewhere shows that all residues are labeled as $^{13}C'$ (although to different degrees) with the exception of His and Leu that are not labeled and that labeling at ^{13}C is under 2%. A 17-residue fragment (KKTKPTPPPKPSHLKPK) from the yeast protein Ark1p peptide[14] was expressed and purified as described previously[13]; the peptide was unlabeled. A 1.4 mM protein sample was prepared, 50 mM sodium phosphate, 100 mM NaCl, 1 mM EDTA, 1 mM NaN_3 pH 7.0 and subsequently titrated with peptide such that the mole fraction of the bound state is 7% (established by relaxation dispersion measurements). After experiments were performed on the isotropic sample, ~ 46 mg/ml Pf1 phage[15], purchased from ASLA biotech, was added (residual ^{2}H water splitting of ~ 55 Hz; ^{15}N-^{1}HN dipolar couplings ranging from –28 to 17 Hz) and measurements repeated (see below). A second sample was prepared, identical to the first, with the exception that the protein concentration was 0.2 mM and the protein was fully bound with peptide. To this sample was added ~ 32 mg/ml Pf1 phage (residual ^{2}H water splitting of ~ 38 Hz; ^{15}N-^{1}HN dipolar couplings ranging from –32 to 30 Hz) after experiments in the isotropic phase were completed.

NMR Data Acquisition and Analysis: $^{13}C'$-relaxation dispersion experiments were recorded on isotropic and phage loaded samples of the ^{15}N, $^{13}C'$, ^{2}H-labeled Abp1p SH3 domain in complex

with 7% (by mole fraction) Ark1p peptide. Experiments were performed at 25ºC on Varian spectrometers operating at 500 and 800 MHz (^{1}H frequency) equipped with room temperature triple resonance probe-heads. A pulse scheme similar to that proposed by Ishima *et al*[16] for measuring ^{13}C'-relaxation dispersion profiles was employed with a number of differences, as illustrated in Supplementary Figure 1. 18 values of ν_{CPMG} (see below) ranging from 33 to 1000 Hz (T_{relax} = 30 ms) were recorded on the isotropic sample (*i.e.*, no alignment), with a pair of values repeated for estimation of errors in relaxation rates. Relaxation dispersion profiles were based on measuring times of 25 (500 MHz) and 15 hours (800 MHz). After completion of experiments in the isotropic phase Pf1 was added to the sample, as described above, and further experiments were performed on an aligned system. Dispersion profiles for the oriented sample were based on 15 values of ν_{CPMG} ($33 \leq \nu_{CPMG} \leq 1$KHz), along with a pair of repeats for error analysis. Acquisition times of 41 and 34 hours were employed for data obtained at 500 and 800 MHz respectively.

Data sets were processed and analyzed with the NMRPipe program[17] and signal intensities quantified using the program FuDA (smk@kiku.dk). Relaxation dispersion profiles, $R_{2,eff}(\nu_{CPMG})$, were generated from peak intensities, $I_1(\nu_{CPMG})$, in a series of 2D ^{1}HN-^{15}N correlation maps measured as a function of CPMG frequency[18], $\nu_{CPMG} = 1/(4\tau_{CP})$, where $2\tau_{CP}$ is the interval between consecutive refocusing pulses of the CPMG sequence. Peak intensities were converted into effective relaxation rates via $R_{2,eff}(\nu_{CPMG}) = -1/T_{relax} \cdot \ln(I_1(\nu_{CPMG})/I_0)$, where I_0 is the peak intensity in a reference spectrum recorded without the relaxation delay T_{relax}.

Values of the exchange rate, the population of the invisible state, chemical shift differences between states and intrinsic relaxation rates were extracted using in-house written software by minimization of the following ^{2} target function:

$$^{2}(\ ) = \frac{\left(R_{2,\mathrm{eff}}^{\mathrm{clc}}(\ ) \quad R_{2,\mathrm{eff}}^{\mathrm{exp}}\right)^{2}}{\left(\ R_{2,\mathrm{eff}}^{\mathrm{exp}}\right)^{2}}, \qquad (1)$$

where $R_{2,\mathrm{eff}}^{\mathrm{exp}}$ and $R_{2,\mathrm{eff}}^{\mathrm{exp}}$ are experimental effective relaxation rates and their uncertainties, respectively, $R_{2,\mathrm{eff}}^{\mathrm{clc}}(\ )$ are model relaxation rates obtained by numerical integration of the Bloch-McConnell equations[19] for a two-site chemical exchange model, denotes the set of adjustable model parameters and the summation in eq 1 is over the number of experimental data points. Dispersion profiles from separate residues recorded at 500 and 800 MHz were analyzed together to extract exchange parameters and shift differences, ^{iso} and ^{aniso}. Dispersion profiles were not included in subsequent analyses if (i) | | < 0.1 ppm (in all cases the two-site model generated statistically significant improvements in fits over a model of no exchange at the 98% confidence level) or (ii) if the reduced ^{2} value for fits of an individual profile > 1.5 (isotropic sample) or 2 (aligned). In total 18 (unaligned sample) and 14 (oriented sample) residues were retained for subsequent analysis.

Signs of chemical shift differences cannot be obtained by analysis of relaxation dispersion data sets. However, they can be measured by the method of Skrynnikov *et. al*.[20] In this approach, ^{1}HN-^{13}C' data sets were obtained at 500 and 800 MHz with ^{13}C' chemical shift recorded either from evolution of single-quantum (HSQC-type) or multiple-quantum (^{15}N-^{13}C' HMQC-type) coherences and the position of correlations compared in (i) HMQC and HSQC maps obtained at 500 MHz, (ii) HMQC and HSQC maps obtained at 800 MHz and (iii) HSQC maps generated at 500 and 800 MHz. In the few cases where conflicting results were obtained via (i)-(iii) the sign was based on the comparison that showed the largest difference in peak positions. For values of | |< 0.1 ppm signs could not obtained reliably (manuscript in preparation) and for this reason a shift difference of 0.1 ppm was used as a cutoff (see above).

Best fit values of $p_B = [PL]/([P]+[PL])$ and $k_{ex} = k_{on}[L] + k_{off}$, obtained from fits of dispersion data recorded on unaligned and aligned samples are (7.5%,247s^{-1}) and (6.9%,271s^{-1}), respectively, with extracted values of ^{iso} and ^{aniso} listed in Supplementary Table 1. Values of $_A$ were obtained by a comparison of peak positions (in the ^{13}C' dimension) in ^{13}C'-^{1}HN planes of HNCO data sets[21] that were recorded on the 7% peptide-bound sample both in the absence and presence of alignment. Values of $_B$ were obtained similarly using a fully ligand bound, dilute sample described above (direct method) or, in the case of the invisible excited state, by the procedure summarized in Figure 1c.

References

(1) Geen, H.; Freeman, R. *J. Magn. Reson.* **1991**, *93*, 93-141.

(2) Muller, L.; Legault, P.; Pardi, A. *J Am Chem Soc* **1995**, *117*, 11043-11048.

(3) Mulder, F. A.; Spronk, C. A. E. M.; Slijper, M.; Kaptein, R.; Boelens, R. *J. Biomol. NMR* **1996**, *8*, 223-238.

(4) Gullion, T.; Baker, D. B.; Conradi, M. S. *J. Magn. Reson.* **1990**, *89*, 479-484.

(5) Shaka, A. J.; Keeler, J.; Frenkiel, T.; Freeman, R. *J. Magn. Reson.* **1983**, *52*, 335-338.

(6) Kay, L. E.; Keifer, P.; Saarinen, T. *J. Am. Chem. Soc.* **1992**, *114*, 10663-10665.

(7) Schleucher, J.; Sattler, M.; Griesinger, C. *Angew. Chem. Int. Ed. Engl.* **1993**, *32*, 1489-1491.

(8) Marion, D.; Ikura, M.; Tschudin, R.; Bax, A. *J. Magn. Reson.* **1989**, *85*, 393-399.

(9) Yang, D.; Venters, R. A.; Mueller, G. A.; Choy, W. Y.; Kay, L. E. *J. Biomol. NMR* **1999**, *14*, 333-343.

(10) Rath, A.; Davidson, A. R. *Protein Sci* **2000**, *9*, 2457-2469.

(11) Lila, T.; Drubin, D. G. *Mol Biol Cell* **1997**, *8*, 367-385.

(12) Drubin, D. G.; Mulholland, J.; Zhu, Z. M.; Botstein, D. *Nature* **1990**, *343*, 288-290.

(13) Vallurupalli, P.; Hansen, D. F.; Stollar, E. J.; Meirovitch, E.; Kay, L. E. *Proc Natl Acad Sci U S A* **2007**, *104*, 18473-18477.

(14) Haynes, J.; Garcia, B.; Stollar, E. J.; Rath, A.; Andrews, B. J.; Davidson, A. R. *Genetics* **2007**, *176*, 193-208.

(15) Hansen, M. R.; Mueller, L.; Pardi, A. *Nat. Struct. Biol.* **1998**, *5*, 1065-1074.

(16) Ishima, R.; Baber, J.; Louis, J. M.; Torchia, D. A. *J Biomol NMR* **2004**, *29*, 187-198.

(17) Delaglio, F.; Grzesiek, S.; Vuister, G. W.; Zhu, G.; Pfeifer, J.; Bax, A. *J. Biomol. NMR* **1995**, *6*, 277-293.

(18) Mulder, F. A. A.; Skrynnikov, N. R.; Hon, B.; Dahlquist, F. W.; Kay, L. E. *J. Am. Chem. Soc.* **2001**, *123*, 967-975.

(19) McConnell, H. M. *J. Chem. Phys.* **1958**, *28*, 430-431.

(20) Skrynnikov, N. R.; Dahlquist, F. W.; Kay, L. E. *J. Am. Chem. Soc.* **2002**, *124*, 12352-12360.

(21) Kay, L. E.; Ikura, M.; Tschudin, R.; Bax, A. *J. Magn. Reson.* **1990**, *89*, 496-514.